

MICROMACHINED MEMBRANE PARTICLE FILTERS

X. Yang, J. M. Yang*, X. -Q. Wang, E. Meng, Y. -C. Tai, and C. -M. Ho*

Caltech Micromachining Laboratory
Electrical Engineering, 136-93
California Institute of Technology
Pasadena, CA 91125, USA

*Department of Mechanical and Aerospace Engineering
University of California, Los Angeles
Los Angeles, CA 90095, USA

ABSTRACT

We report here several particle membrane filters ($8 \times 8 \text{ mm}^2$) with circular, hexagonal and rectangular through holes. By varying hole dimensions from 6 to 12 μm , opening factors from 4 % to 45 % are achieved. In order to improve the filter robustness, a composite silicon nitride/Parylene membrane technology is developed. A more than 4 times higher burst pressure has been achieved with 2.69 μm Parylene deposition. Fluid dynamical performance of the filters has been studied extensively through experiments and numerical simulations. It is shown that the gaseous flow in filters strongly depends on opening factors. Furthermore, the measured pressure drops are much lower in comparison to numerical simulation results. Surface velocity slip can only account for a minor part of the difference. This discrepancy suggests a very interesting topic for basic fluid mechanics research.

INTRODUCTION

Filtering and collecting of particles is a fundamental process in airborne particle sampling. As the dimensions of the airborne particles fall in the range of 1 to 10 μm [1], a micromachined membrane with perforations is an ideal candidate for such filters. Although several filters [2,3,4] have been reported in the past, comprehensive study of their strength and performance is not available.

The requirements for these particle filters are, first, they must be mechanically robust. Second, as high detection sensitivity of particle sampling requires a large amount of air filtered per unit time, the flow rate of the filters must necessarily be high. Third, the pressure drop, and hence the power requirement to sustain a desired flow rate, has to be low.

Many factors including hole dimension, shape, membrane thickness and the opening area factor ($b = \text{area of holes}/\text{total area}$) can affect the pressure drop,

flow rate and the strength of the filters. Large holes and large opening factor will decrease the pressure drop and increase the flow rate, but the strength of the membrane will be also decreased. Different hole shapes will not only change the flow rate and pressure drop, but also change the stress concentration level in the membrane, and hence the strength of the filter. The goal of this project is to develop new structure and fabrication process to enhance the strength of the filters, and to establish a guideline to design an optimal filter by studying the fluid dynamical performance experimentally and numerically.

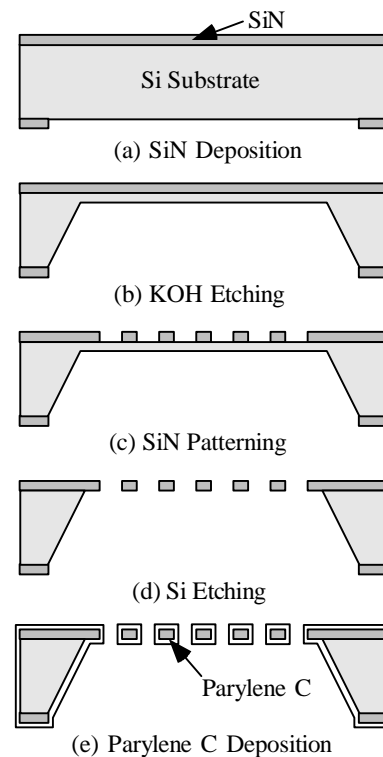
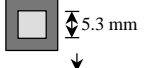
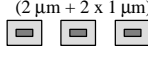
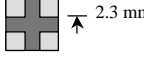
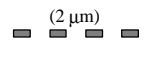
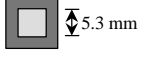
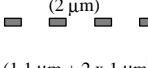

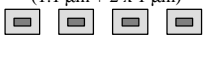

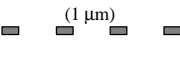

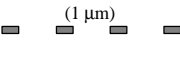

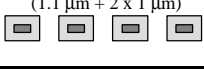


Fig. 1 Fabrication Process

Table 1 Filter Design

Filter	Top View (8 mm x 8 mm)	Cross-sectional View	Hole Size d (μm) or a × b (μm ²)	Opening Factor β (%)	Hole Shape
	■ : Non-Filtering Area □ : Filtering Area	■ : Silicon Nitride □ : Parylene Coating			
1			6	4	Circular
2			8 ~ 8.8	8	Circular
3			10.6	13	Circular
4			8	20	Hexagonal
5			12	45	Hexagonal
6			5 × 20	39	Rectangular
7			3 × 18	21	Rectangular

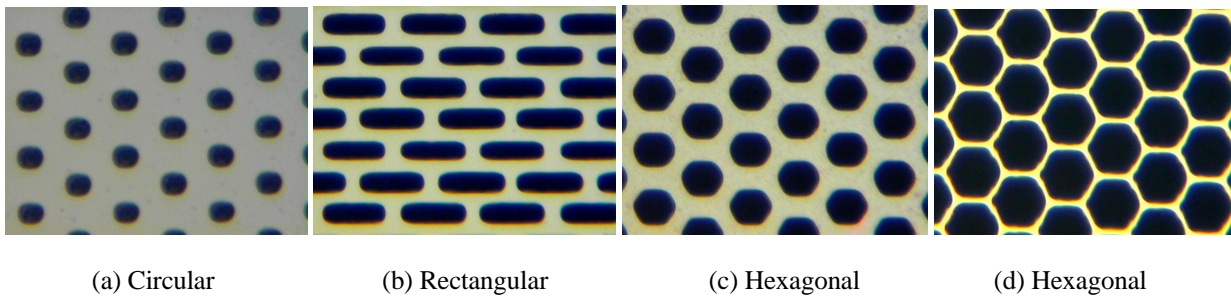


Fig. 2 Microphotographs of the Fabricated Filters

FABRICATION

The filters are fabricated by using the process shown in Fig. 1. First, a layer of 1 μm thick LPCVD silicon nitride (SiN) is deposited at 850 °C with a SiH₂Cl₂:NH₃ gas flow ratio of 4:1 to achieve low stress [5]. Windows on the backside of the wafers are opened using plasma etching. The wafers are then etched in potassium hydroxide (KOH) until only 20 μm silicon is left. Next, an array of filtering holes is etched into the silicon nitride layer on the front side of the wafer using reactive ion etching (RIE). Then the wafers are diced and etched in KOH again to remove the silicon layer and free the membrane. By dicing the wafers before the membranes are freed, the possibility of damaging the membranes during the dicing is avoided. Finally, a layer of polymer poly-p-xylylene (Parylene C, Specialty Coatings Systems) is deposited conformally over the wafers or individual dies. This layer of Parylene layer serves two purposes. First, it can greatly improve the strength of the membrane filters. Second, since the Parylene

deposition is uniform, different hole sizes can be obtained from the same basic filter by varying the thickness of the Parylene layer.

DESIGN

With the above fabrication process, several membrane filters as large as 8 × 8 mm² have been fabricated. The membrane filters are perforated with various shapes of holes such as circular, rectangular and hexagonal. As shown in Table 1, the opening factor of the filters is in the range of 4 % to 45 % with different hole sizes and pitches. As shown in testing section later, the pressure drop, power requirement of the filters to sustain a desired flow rate strongly depend on the opening factor. This means a high opening factor is preferred in order to achieve low pressure drop and high flow rate in the filters. It is obvious that the opening factor increases as the hole size increases. However, the hole size can not be too large because the hole size defines the filtering threshold which is the minimum size of the particles

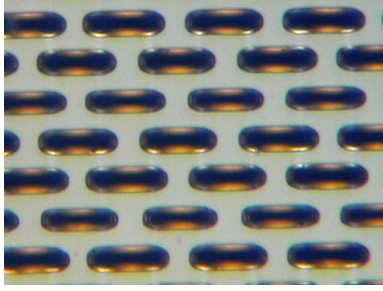


Fig. 3 Microphotograph of a Parylene Coated Filter 6 in Fig. 2 (b)

Table 2 Filter Strength
(Filter 6, $\beta = 39\%$)

Parylene Thickness (μm)	Burst Pressure (PSI)
0	0.9
1.38	1.9
2.69	4.2

that can be collected by the filters. For example, filters with $10.6\ \mu\text{m}$ diameter circular holes have an opening factor of 13 %. Hexagonal holes can give higher opening factor than circular holes, but they cause higher stress concentration in the membrane, which decreases the strength of the filters. Rectangular holes can give a large range of opening factors without changing the filtering threshold as long as one dimension of the rectangular holes is kept constant. But they suffer from the same problem of stress concentration as hexagonal holes. In Fig. 2 are photographs of the fabricated filters with (a) circular (b) rectangular and (c, d) hexagonal holes.

STRENGTH

Since the filters will be used for particle collection, they have to be strong enough to stand the aerodynamic load. The strength of the filters is measured. For comparison, the strength of flat silicon nitride membranes with identical thickness and dimensions but no perforations is also measured.

High pressure air flow is passed through the filters. By increasing the flow until the filter breaks, the burst pressure is measured using a pressure transducer. For example, a $1\ \mu\text{m} \times 8\ \text{mm} \times 8\ \text{mm}$ membrane bursts at 5.5 psi while a Filter 6 (Fig. 2 (b)) in Table 1 bursts at 0.9 psi. Filter 6 has a lower burst pressure due to the stress concentration in the membrane caused by the perforations. As mentioned earlier, a layer of Parylene is conformally deposited on the filters to improve the strength. Fig. 3 is a picture of a Filter 6 coated with $1.38\ \mu\text{m}$ of Parylene. The shadows around every hole clearly show the conformal nature of the Parylene deposition. Table 2 shows that with $2.69\ \mu\text{m}$ thick Parylene deposition, the burst pressure of Filter 6 is increased to 4.2 psi which is more than four times that of an uncoated one.

TESTING

To test the fluid dynamical performance, a small wind tunnel shown in Fig. 4 is designed and built. The wind tunnel consists of inlet, settling chamber, contraction, testing chamber, diffuser and suction fan. A prefilter is inserted at the inlet of the wind tunnel to prevent the unwanted particles in the air from clogging the filter under test. The contraction section is carefully designed so that a uniform mean flow in the test section can be achieved and there is no separation of the flow at the inlet of the test section. Several different commercial suction fans (computer fan, hair dryer fan, etc.) are used to provide flow up to $100\ \text{liter}/\text{min}/\text{cm}^2$. The test section has a length of 30 cm and a cross-section of 8 mm by 8 mm. The filter is tested at the point 15 cm downstream

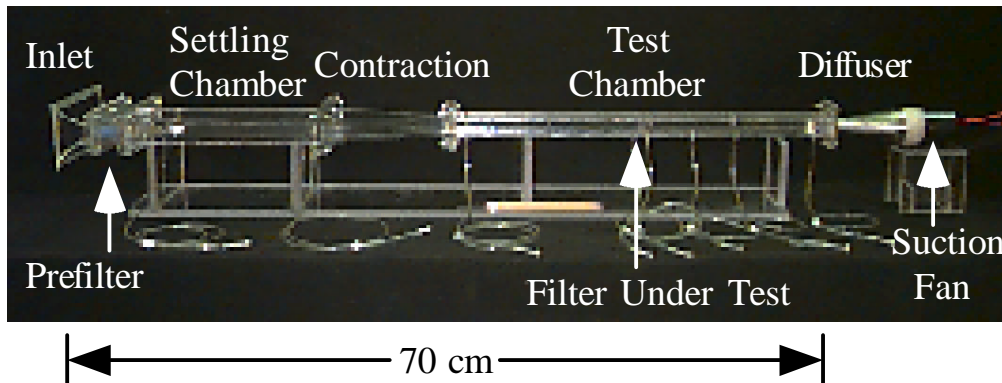


Fig. 4 Wind Tunnel Testing Setup

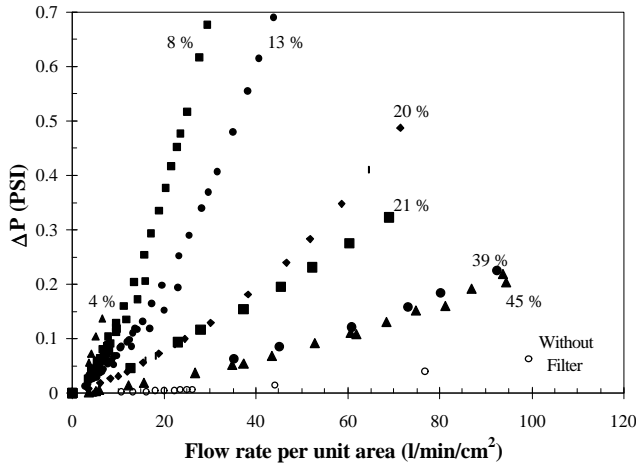


Fig. 5 Pressure Drop Vs. Flow Rate per Unit Area of Filters with Different Opening Factors

from the contraction. Pressure drop across the filters is measured by using a manometer which has a resolution of 0.005 mmHg. The flow rate is measured by Venturi tube principle. By measuring static pressure before the contraction (P_1) and after the contraction (P_2) of the wind tunnel using a MKS Baratron differential pressure transducer and solving the continuity equation,

$$U_1 A_1 = U_2 A_2 \quad (1)$$

and the Bernoulli equation,

$$P_1 + \frac{\rho U_1^2}{2} = P_2 + \frac{\rho U_2^2}{2} \quad (2)$$

the volumetric flow rate Q can be calculated as

$$Q = U_2 A_2 = A_2 \sqrt{\frac{2(P_1 - P_2)}{\rho \left(1 - \frac{A_2^2}{A_1^2}\right)}} \quad (3)$$

Pressure drop as a function of the flow rate per unit area for seven different filters is plotted in Fig. 5. The power required to sustain a desired flow rate is calculated by multiplying the pressure drop by the volumetric flow rate and the result is shown in Fig. 6. It can be seen that the pressure drop and the power requirements strongly depend upon the opening factor of the filter.

NUMERICAL CALCULATION

One of the goals of this project is to establish a design guide for membrane filters. As seen from the filter testing, the pressure drop and the power requirement depend upon the dimension (d) and shape of the holes and the thickness of membrane (t) as well as the filter

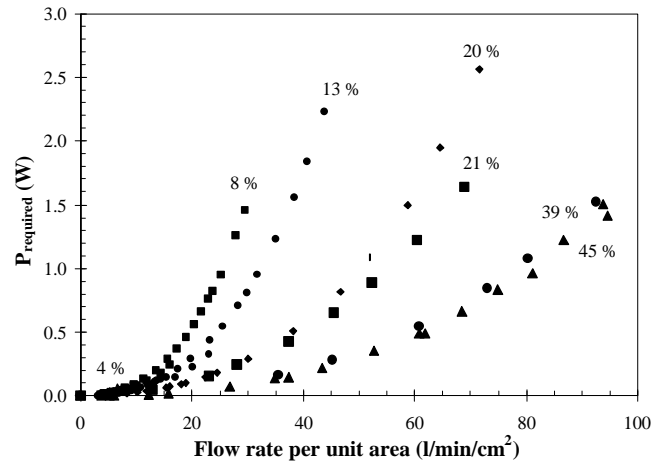


Fig. 6 Power Requirement Vs. Flow Rate Per Unit Area of Filters with Different Opening Factors

opening factors (b). In non-dimensional analysis, this can be shown as,

$$K = \frac{\Delta P}{\frac{1}{2} \rho U_{in}^2} = f(\text{Re}, b, t/d), \quad (4)$$

where K is the pressure coefficient, Re is the Reynolds number and is defined as

$$\text{Re} = \frac{U_h d}{\nu}, \quad (5)$$

where U_h is the average velocity across the hole, d is the diameter of the hole and ν is the kinematic viscosity of air. In our filter testing experiments, Re is in the range of 1 to 40.

Wieghardt [6] and Schubauer, *et al* [7] proposed empirical formulas for K , but their formulas are only valid for large Reynolds number flow ($\text{Re} > 60$) and large holes ($d > 100 \mu\text{m}$). Recently, Hasegawa *et al.* [8] investigated the pressure drop through a single orifice as small as $8.8 \mu\text{m}$. However, all the testing were done with liquid. Therefore, none of the existing empirical formulas can model the fluid behavior in our membrane filters. Numerical simulation is sought to establish the empirical formula for the micromachined membrane filters with small holes and operated in low Reynolds number flow regime.

Considering that the filter can be regarded as an array of small holes, we perform numerical calculation around a single axis-symmetric cylindrical orifice by using the following model in CFDRC (Computational Fluid Dynamics Research Corporation) software.

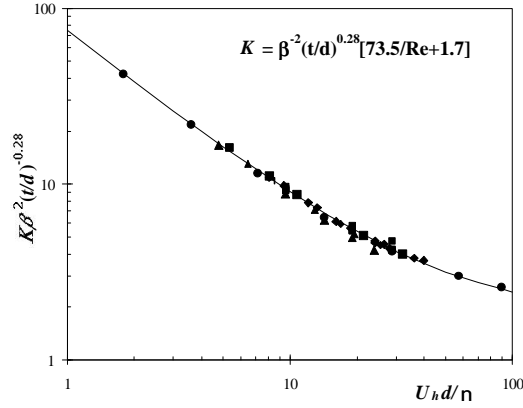


Fig. 7 Numerical Calculation for Various Geometric Factors

By assuming no-slip boundary condition at the surface of the filter, viscous laminar flow and varying the following parameters,

$$10\% < \beta < 45\%$$

$$0.08 < t/d < 0.5$$

$$1 < Re < 100$$

the pressure drop is calculated and plotted in Fig. 7. It is found that the results can be plotted into a single curve regardless of the geometrical parameters if the following non-dimensional form is used.

$$K b^2 \left(\frac{t}{d}\right)^n = f\left(\frac{U_h d}{n}\right) \quad (6)$$

As shown in Fig. 7, fitting the curve results in the following empirical formula.

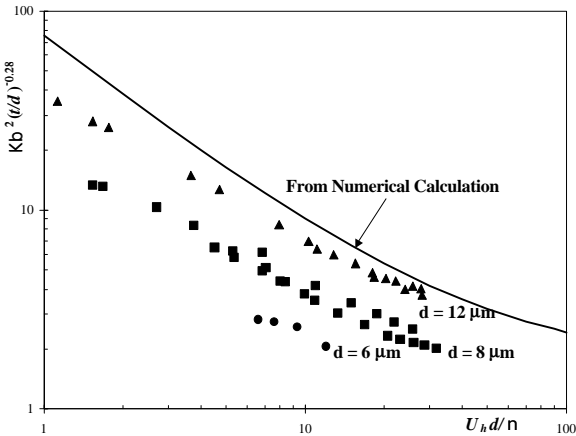


Fig. 8 Experiments Vs. Numerical Calculations

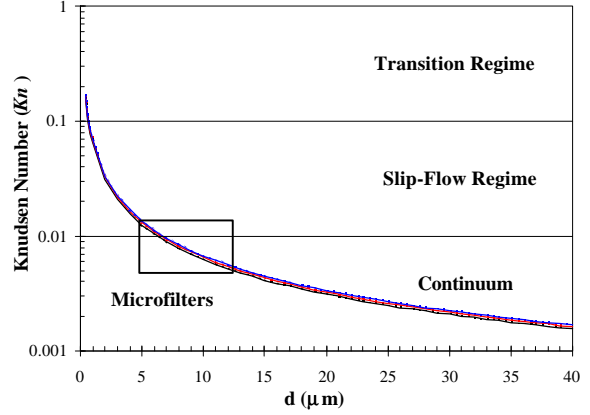


Fig. 9 Knudsen Number Vs. Filter Hole Size

$$K = \frac{\Delta P}{\frac{1}{2} \rho U_{in}^2} = b^{-2} \left(\frac{t}{d}\right)^{0.28} \left[73.5 \frac{n}{U_h d} + 1.7\right] \quad (7)$$

As equation (7) shows that the pressure drop coefficient depends on the 2nd power of the opening factor b, it can be concluded that the opening factor is the most important parameter in determining the pressure drop, which is consistent with the results shown in Fig.5.

RESULTS AND DISCUSSION

To make sure the empirical equation is valid, the numerical calculation has to be compared with experimental results. Plotted in Fig. 8 are pressure drop coefficient from the empirical formula and pressure drop coefficient of filters with 6 μm , 8 μm , 12 μm holes from experiments. It can be seen that there is larger difference as the dimension of the hole becomes smaller. This indicates that some of the assumptions that are used in the numerical calculation are no longer valid. Since the filter holes are very small, one possibility is the no-slip boundary condition. The common way to check the possibility of slip at the wall is to calculate the Knudsen number (Kn) of the flow field. Knudsen number is defined as the ratio of the mean free path (λ) of working fluid (air in this case, $\lambda = 0.0685 \mu\text{m}$ at 1atm) to the physical dimension of flow field (hole size, d , in the case). It is well known that slip occurs at the wall if the Knudsen number is larger than 0.01. The Knudsen number as a function of the hole size of the filters is plotted in Fig. 9. It is shown that Knudsen number of the filters ranges from 0.005 to 0.015. The Knudsen number in the case of $d = 8 \mu\text{m}$ is approximately 0.009, which means that slip could occur.

To check if it really is no-slip boundary condition that causes the big discrepancy between numerical calculation and experiments, more numerical calculation

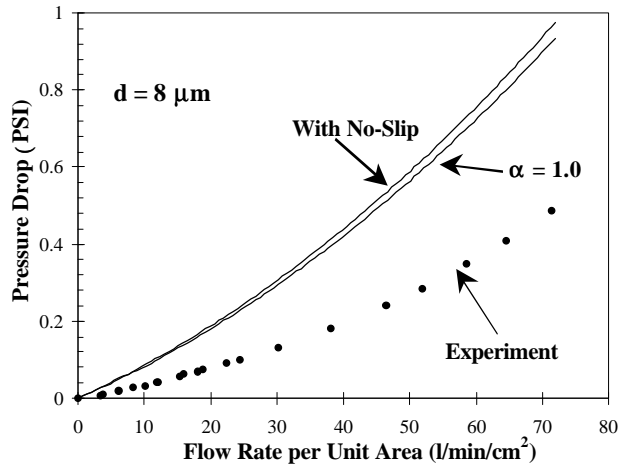


Fig. 10 Numerical Calculation Results with Slip Boundary Condition

is done by including the following slip boundary condition,

$$u_w = \pm \frac{2-a}{a} \lambda \left. \frac{du}{dy} \right|_w \quad (8)$$

where α is the accommodation constant that is in the range from 0 to 1 and λ is the mean free path of air. The result is shown in Fig. 10. Even though the slip boundary condition is included and α is varied between 0 and 1, there is still a large difference. This suggests that some other mechanisms must be involved. For example, in numerical calculation, no consideration is given to surface roughness and interaction between the wall surface molecules and the molecules in the air flow. Also, to simplify the simulation process, the hole and boundary between holes are assumed to be circular even though the real shape of the filter hole is hexagonal. So far, no specific mechanism has been identified to explain the discrepancy. More work is underway to determine which one or both of them are responsible.

CONCLUSION

We have designed, fabricated and tested several particle membrane filters ($8 \times 8 \text{ mm}^2$) with circular, hexagonal and rectangular filtering holes. By varying hole dimensions from 6 to $12 \mu\text{m}$, opening factors from 4 % to 45 % are achieved. In order to improve the filter robustness, a composite silicon nitride/Parylene membrane technology is developed. Fluid dynamical performance of the filters has been studied extensively through experiments and numerical simulations. It is found that the gaseous flow in filters strongly depends on opening factors. Furthermore, the measured pressure drops are much lower in comparison to numerical simulation results. Numerical calculation with slip

boundary condition shows that surface velocity slip can only account for a minor part of the difference. More work is underway to find out the mechanism that causes this discrepancy.

ACKNOWLEDGMENTS

This work is supported by the DARPA MICRO-FLUMES program under Naval Ocean Systems Center Contract N66001-96-C-83632. The authors would like to thank Trevor Roper for help with processing.

REFERENCES

- [1] C. N. Davies, "Aerosol Science", Academic Press, 1966, pp. 409.
- [2] C. J. M. van Rijn, and M. C. Elwenspoek, "Micro Filtration Membrane Sieve with Silicon Micro Machining for Industrial and Biomedical Applications", Proceedings of IEEE the Eighth Workshop on Micro Electro Mechanical Systems, 1995, pp. 83-87.
- [3] C. J. M. van Rijn, M. van der Wekken, W. Nijdam, and M. C. Elwenspoek, "Deflection and Maximum Load of Microfiltration Membrane Sieves Made with Silicon Micromachining", Journal of Microelectromechanical Systems, Vol. 6, No.1, March, 1997, pp. 48-54.
- [4] G. Kittilsland, G. Stemme, and B. Norden, "A Submicron Particle Filter in Silicon", Sensors and Actuators (A:Physical), Vol. 23 (1-3), 1990, pp.904-907.
- [5] M. Sekimoto, H. Yoshihara, and T. Ohkubo, "Silicon Nitride Single-Layer X-Ray Mask", Journal of Vacuum Science and Technology, Vol.21(4), November/December, 1982, pp.1017-1021.
- [6] K. E. G. Wieghardt, "On the Resistance of Screens", The Aeronautical Quarterly, Vol. IV, February, 1953, pp.186-192.
- [7] G. B. Schubauer, W. G. Spangenberg, P. S. Klebanoff, "Aerodynamic Characteristics of Damping Screens", N. A. C. A., Technical Notes 2001, 1950.
- [8] T. Hasegawa, M. Suganuma, and H. Watanabe, "Anomaly of Excess Pressure Drops of the Flow Through Very Small Orifices", Physics of Fluids, Vol. 9, No.1, January 1997, pp. 1-3.